

Conformation and Dynamics of Abasic Sites in DNA Investigated by Time-Resolved Fluorescence of 2-Aminopurine[†]

Edward L. Rachofsky,[‡] Eleanore Seibert,[‡] James T. Stivers,[§] Roman Osman,^{||} and J. B. Alexander Ross^{*‡}

Department of Biochemistry and Molecular Biology and Department of Physiology and Biophysics, Mount Sinai School of Medicine, New York, New York 10029, and Center for Advanced Research in Biotechnology, Biotechnology Institute, University of Maryland, National Institute of Standards and Technology, Rockville, Maryland 20850

Received July 17, 2000; Revised Manuscript Received October 30, 2000

ABSTRACT: Abasic sites are highly mutagenic lesions in DNA that arise as intermediates in the excision repair of modified bases. These sites are generated by the action of damage-specific DNA glycosylases and are converted into downstream intermediates by the specific activity of apurinic/apyrimidinic endonucleases. Enzymes in both families have been observed in crystal structures to impose deformations on the abasic-site DNA, including DNA kinking and base flipping. On the basis of these apparent protein-induced deformations, we propose that altered conformation and dynamics of abasic sites may contribute to the specificity of these repair enzymes. Previously, measurements of the steady-state fluorescence of the adenine analogue 2-aminopurine (2AP) opposite an abasic site demonstrated that binding of divalent cations could induce a conformational change that increased the accessibility of 2AP to solute quenching [Stivers, J. T. (1998) *Nucleic Acids Res.* 26, 3837–44]. We have performed time-resolved fluorescence experiments to characterize the states involved in this conformational change. Interpretation of these studies is based on a recently developed model attributing the static and dynamic fluorescence quenching of 2AP in DNA to aromatic stacking and collisional interactions with neighboring bases, respectively (see the preceding paper in this issue). The time-resolved fluorescence results indicate that divalent cation binding shifts the equilibrium of the abasic site between two conformations: a “closed” state, characterized by short average fluorescence lifetime and complex decay kinetics, and an “open” state, characterized by monoexponential decay with lifetime approximately that of the free nucleoside. Because the lifetime and intensity decay kinetics of 2AP incorporated into DNA are sensitive primarily to collisional interactions with the neighboring bases, the absence of dynamic quenching in the open state strongly suggests that the fluorescent base is extrahelical in this conformation. Consistent with this interpretation, time-resolved quenching studies reveal that the open state is accessible to solute quenching by potassium iodide, but the closed state is not. Greater static quenching is observed in the abasic site when the fluorescent base is flanked by 5′- and 3′-thymines than in the context of 5′- and 3′-adenines, indicating that 2AP is more stacked with the neighboring bases in the former sequence. These results imply that the conformation of the abasic site varies in a sequence-dependent manner. Undamaged sequences in which the abasic site is replaced by thymine do not exhibit an open state and have different levels of both static and dynamic quenching than their damaged homologues. These differences in structure and dynamics may be significant determinants of the high specific affinity of repair enzymes for the abasic site.

DNA abasic sites arise at a high frequency in living cells both spontaneously and as intermediates in the base excision repair (BER)¹ of damaged or modified bases (1, 2). The abasic site is labile, being vulnerable to reactions leading to both single-stranded and double-stranded breaks in DNA and

consequently is highly mutagenic (3, 4). In BER, abasic sites are created by the cleavage of the glycosidic bond between a modified base and the backbone deoxyribose. This reaction is catalyzed for each type of damaged base by a damage type-specific DNA glycosylase (5, 6). Both spontaneously arising and enzyme-generated abasic sites are resolved by enzymatic cleavage of the phosphodiester bond 5′ to the abasic sugar by an apurinic/apyrimidinic (AP) endonuclease (6, 7). The product of this reaction subsequently undergoes a series of further enzymatic steps of which the ultimate product is undamaged DNA.

Both damage-specific DNA glycosylases and AP endonucleases demonstrate high affinity for abasic sites (8–10). In the case of the glycosylases, it has been proposed that this binding affinity exists because the bound enzyme protects the abasic site from chemical or enzymatic reactions resulting

[†] Support: NSF Grant DBI-9724330 and NIH Grant CA63317.

^{*} To whom correspondence should be addressed. Telephone: (212) 241–5569. Fax: (212) 996-7214. E-mail: ross@inka.mssm.edu.

[‡] Department of Biochemistry and Molecular Biology, Mount Sinai School of Medicine.

[§] University of Maryland, NIST.

^{||} Department of Physiology and Biophysics, Mount Sinai School of Medicine.

¹ Abbreviations: base excision repair, BER; 2AP, 2-aminopurine; d2AP, 2-amino-9-deoxyribosylpurine; UDG, *Escherichia coli* uracil DNA glycosylase; AlkA, *E. coli* alkylated base glycosylase; endo IV, *E. coli* endonuclease IV; HAP1, human apurinic/apyrimidinic endonuclease I; endo V, bacteriophage T4 endonuclease.

in strand-cleaved products (11). In contrast, the AP endonucleases require specific high-affinity binding to differentiate their substrate sites from the vast excess of undamaged DNA present in the cell. For both classes of enzyme, it has been proposed that high-affinity binding to this damaged site arises in part from the susceptibility of the abasic site to particular structural deformations, including DNA kinking and “flipping” of both the abasic sugar and the opposite base (12, 13). These hypotheses have been suggested by structural studies of abasic site-repair enzyme complexes that show such deformations (as reviewed below). However, no direct measurement of the conformational flexibility of the abasic site in solution has been reported. In this study, we utilize the fluorescence of an incorporated base analogue, 2-aminopurine, to probe the conformation and dynamics of abasic site DNA.

Numerous structural studies of abasic site DNA have been performed by nuclear magnetic resonance (NMR) methods (14–26). The species studied have included the 2′-deoxyribose abasic site that is generated in BER (14–20, 23, 25, 26), the chemically stable tetrahydrofuran (THF) analogue of this site (21, 22), and the alternative 2′-deoxyribonolactone site (24), which is produced in vivo by some types of chemical damage. Investigations of the 2′-deoxyribose site have revealed that the abasic sugar exists as an equilibrium mixture of α - and β -hemiacetals, indicating that there is some conformational heterogeneity at this site (20, 26). A single study indicated that the base opposite the abasic site was sometimes found in an extrahelical conformation or in a mixture of extrahelical and intrahelical conformations, depending on the identity of the base (14). However, the majority of the reported structures of abasic species have revealed none of the gross deformations—DNA kinking, deoxyribose flipping, opposite-base flipping—that are observed in complex with repair enzymes.

Four different complexes between a repair enzyme and an abasic site have been determined by X-ray crystallography. The enzymes include *Escherichia coli* uracil DNA glycosylase (UDG) (27), *E. coli* alkylated-base glycosylase AlkA (28), *E. coli* endonuclease IV (endo IV) (29), and human AP endonuclease I (HAP1, APE1, or ref 1) (30). The structures of the abasic-site DNA in these complexes display both common and unique features. In all four protein–DNA complexes, the DNA is sharply kinked at the damaged site, with accompanying compression of the major groove. In each case, kinking appears to allow binding contacts to be formed between the protein and the phosphate backbone 5′ and 3′ to the abasic site. However, the local DNA conformation is unique to each enzyme.

UDG is the prototypical damage-specific repair glycosylase, which exists to remove uracil from DNA (5). In complex with UDG, uracil “flips” out of the DNA helix and into a cavity within the protein that contains the catalytic residues. The structure of UDG complexed with a noncleavable substrate analogue demonstrates DNA kinking, flipping of the abasic sugar, and flipping of the opposite base (31). The abasic site is the product of the glycosidic cleavage catalyzed by UDG. The affinity of UDG for the abasic product is in the micromolar range (9), and the product complex has been reported to dissociate slowly, with a rate constant of 0.2 s^{-1} at 15°C (11). The DNA is kinked in this complex, with the abasic sugar in a flipped-out conformation

and the opposite base intrahelical (27). Similar features are observed in the complex of the alkylated-base glycosylase AlkA with its product abasic site: in this structure, the DNA is kinked, the abasic deoxyribose is flipped-out, and the opposite base is intrahelical (28).

Endo IV and HAP1 typify the two known families of AP endonucleases, which are defined by both sequence and structural similarities (2). In both enzyme–abasic site complexes, DNA kinking and flipping of the abasic sugar are observed. In the HAP1 complex, the opposite base is intrahelical (30). However, in the endo IV complex, the base opposite the abasic site also is flipped out of the helix (29). The catalytic residues approach the abasic site through the space vacated by the flipped-out base.

Flipping of the opposite base also has been observed in the cocrystal structure of the bifunctional glycosylase-lyase endonuclease V (endo V) of bacteriophage T4 with its primary substrate, a cyclobutane thymine dimer (32). Endo V, which has no sequence similarity to any other known protein, catalyzes the cleavage of both the glycosidic bond and the 5′-phosphodiester bond of the 5′-residue of a thymine dimer (33). In the cocrystal structure of a catalytically inactive mutant of endo V with its substrate, the DNA is kinked, the adenine opposite the 5′-thymine of the dimer is flipped out of the helix, and the catalytic residues approach the thymine dimer through the space vacated by this base. However, unlike the endo IV complex, in which the flipped-out base makes no binding contacts with the protein, in the endo V complex the extrahelical base sits in a cavity within the enzyme. These features of the endo V substrate complex also may exist in the intermediate state—the complex with the abasic site—and the product complex.

In summary, the structures of repair enzyme–DNA complexes suggest either that the abasic site is intrinsically deformed from the normal helical structure of DNA or that it is readily susceptible to protein-induced deformations. The types of deformation that are observed consistently include DNA kinking, compression of the major groove, abasic-sugar flipping, and in some cases opposite base flipping. In contrast to these highly deformed enzyme–DNA complexes, the majority of NMR structures of abasic sites free in solution reveal no kinking, sugar flipping, or opposite-base flipping, suggesting that the deformations are induced upon binding of the repair enzymes.

Other evidence, however, suggests that the abasic site may undergo some or all of these deformations even in the absence of repair enzymes. One NMR study observed two conformational states that differed at the position of the base opposite the abasic site (14). Features of the proton spectra suggested that these two states represented intrahelical and extrahelical bases. The fractional population of these states differed according to the identity of the opposite base. Consistent with this result, fluorescence measurements of abasic site DNA employing the highly fluorescent adenine analogue 2-aminopurine (2AP) in the position opposite the abasic site have suggested that these sites undergo a conformational change upon binding of divalent cations (9). Addition of Ca^{2+} , Mg^{2+} , or Mn^{2+} to these labeled oligonucleotides induced a large, saturable increase in 2AP fluorescence intensity, with an accompanying increase in the susceptibility to collisional quenching by added acrylamide. These results are consistent with a conformational change

Table 1: Abasic-Site Oligonucleotide Sequences^a

| name | sequence |
|---------|---|
| AFA/TPT | 5'-GCGGCCAAA F AAAAAGCGC/ 5'-GCGCTTTTT P TTTGGCCGC |
| APA/TFT | 5'-GCGGCCAAA P AAAAAGCGC/ 5'-GCGCTTTTT F TTTGGCCGC |
| ATA/TPT | 5'-GCGGCCAAA T AAAAAGCGC/ 5'-GCGCTTTTT P TTTGGCCGC |
| APA/TTT | 5'-GCGGCCAAA P AAAAAGCGC/ 5'-GCGCTTTTT T TTTGGCCGC |

^a F = tetrahydrofuran (THF); P = 2-aminopurine (2AP).

shifting the fluorescent base to an extrahelical position. This conformational state may not be detectable in NMR studies because only a small fractional population of molecules may occupy this state at equilibrium. However, even a 10% population of a base-flipped state would have significant implications for the thermodynamics and kinetics of the interactions of repair enzymes with the abasic site.

To characterize further the conformational states of the abasic site, we have performed steady-state and time-resolved fluorescence measurements of 2AP in abasic-site DNA. The interpretation of fluorescence lifetimes and relative quantum yields in these experiments is based on the model of the quenching interactions of 2AP in DNA that is developed in the preceding paper in this issue. By measuring the fluorescence changes in response to the addition of divalent cations, solute quencher, and UDG, we are able to identify two conformational states: one in which the opposite base is intrahelical and another in which it is extrahelical. Both of these states show significant fractional occupation at all concentrations of divalent ion. This result suggests that repair enzymes such as endo IV may recognize a preexisting deformed state of abasic-site DNA and implies that the lower energetic cost of deforming the damaged site relative to normal DNA may contribute to the specificity of such enzymes.

MATERIALS AND METHODS

Oligonucleotides and Other Materials. Single-stranded 19-mers containing normal DNA bases, 2AP, and THF were synthesized as previously described (9). The sequences of the four double-stranded (ds) oligonucleotides (oligos) employed in this study are listed in Table 1. Oligos are named according to their central three bases: e.g., APA/TTT, where the two three-letter names represent the central sequence read 5' to 3' on each strand. In this one-letter code, 2AP is indicated by P, and the THF abasic site analogue indicated by F. Single-stranded oligos were purified by FPLC on a MonoQ 5/5 column (Pharmacia) using a protocol previously described (34). Peak fractions were collected and concentrated on Centricon 3 spin filters (Millipore). Oligos were annealed by heating a solution of approximately 0.5 mM [ssDNA] to 90 °C for 5 min, then allowing it cool to room temperature over the course of 4–6 h. Double-stranded oligos were separated from excess ssDNA by FPLC on a MonoQ 5/5 column using a similar protocol as for purification of the ss oligos. Absorption spectra were collected for all samples using a Hitachi U-3210 UV/vis dual beam spectrophotometer. Sample concentrations were computed from the absorbance at 303 nm assuming $\epsilon_{303 \text{ nm}} = 6000 \text{ M}^{-1} \text{ cm}^{-1}$ for 2AP in DNA (35). *E. coli* UDG was purified and assayed

as previously described (9). The concentration of UDG was estimated from the UV absorption spectrum assuming $\epsilon_{280 \text{ nm}} = 38\,500 \text{ M}^{-1} \text{ cm}^{-1}$. This extinction coefficient was determined by the LINC method (36). DNA and protein stock solutions were prepared in a buffer of 20 mM tris·HCl, 60 mM NaCl, 0.1 mM Na₂EDTA, with pH adjusted to 7.5 by addition of HCl. Buffer salts were purchased from Sigma and used without further purification.

Titration. Oligos were titrated with divalent cation at constant ionic strength either by serial addition of aliquots of 20 mM tris·HCl, 20 mM CaCl₂, 0.1 mM Na₂EDTA, pH adjusted to 7.5, to oligo samples in the previously described 60 mM NaCl buffer, or by mixing samples in these two buffers that were equal in DNA concentration. For titration with potassium iodide (KI), oligos were prepared in a buffer of 20 mM tris·HCl, 30 mM CaCl₂, 200 mM KCl, and 0.1 mM Na₂EDTA, pH 7.5. KI was introduced by serial additions of a solution of 20 mM tris·HCl, 30 mM CaCl₂, 200 mM KI, and 0.1 mM Na₂EDTA, pH 7.5. The KI stock solution was kept in the dark and contained a small quantity of sodium bisulfite to retard oxidation. New KI stock was prepared each day.

Fluorescence Spectroscopy. Steady-state and time-resolved fluorescence measurements were performed essentially as described in the preceding paper in this issue. Samples were contained in 3 × 10 mm² quartz-windowed fluorescence microcuvettes; these cuvettes enable measurement of samples as small as 50 μL. Relative quantum yields of oligos were estimated by comparison with the fluorescence of 2-aminopurine deoxyribonucleoside (d2AP), which was the gift of Professor Lawrence C. Sowers (City of Hope National Medical Center). The excitation wavelength for all steady-state and time-resolved fluorescence experiments was 309 nm, except as noted below. For determination of relative quantum yields, excitation was at 325 nm to minimize the absorption of the DNA bases. The extinction coefficient for the nucleoside was assumed to be equal to that of 2AP incorporated into DNA. For titrations with UDG, fluorescence excitation was performed at 325 nm to avoid the tryptophan absorption of the protein.

Fluorescence Decay Data Analysis. Time-resolved fluorescence data were analyzed by a standard reconvolution procedure (37) using nonlinear regression (38). The fluorescence intensity decay was fit to a sum of exponentials:

$$I(t) = \sum_{i=1}^n \alpha_i e^{-t/\tau_i} \quad (1)$$

where the preexponential factors α_i are the amplitudes of each component, and τ_i are fluorescence lifetimes. Certain analyses of titration data were performed using a global procedure with lifetimes τ_i as common parameters (39, 40). In cases where a single-exponential term was not adequate to fit the observed kinetics, number-averaged and intensity-averaged fluorescence lifetimes (41) were computed, respectively, according to

$$\tau_{\text{num}} = \frac{\sum_{i=1}^n \alpha_i \tau_i}{\sum_{i=1}^n \alpha_i} \quad (2)$$

$$\tau_{\text{int}} = \sum_{i=1}^n \alpha_i \tau_i^2 / \sum_{i=1}^n \alpha_i \tau_i \quad (3)$$

The value of τ_{num} is proportional to the steady-state fluorescence intensity (in the absence of static quenching). The value of τ_{int} represents the average time that a fluorophore exists in the excited state.

Binding Data Analysis. Binding of Ca^{2+} to oligos was analyzed according to a simple hyperbolic isotherm (42):

$$Y = \frac{K_a[\text{Ca}^{2+}]}{1 + K_a[\text{Ca}^{2+}]} \quad (4)$$

where K_a is the association constant and Y is the fraction of calcium-bound DNA: $[\text{DNA}]_{\text{bound}}/([\text{DNA}]_{\text{bound}} + [\text{DNA}]_{\text{free}})$. This analysis assumes that the interaction of Ca^{2+} with the oligo is a simple two-state process. The bound fraction Y was related to the relative fluorescence F/F_0 according to

$$\frac{F}{F_0} = 1 - Y \left(1 - \frac{\phi_{\text{bound}}}{\phi_{\text{free}}} \right) \quad (5)$$

where F_0 is the fluorescence intensity in the absence of Ca^{2+} , and $\phi_{\text{bound}}/\phi_{\text{free}}$ is the ratio of the relative quantum yields of bound and free states. Because the quantum yields enter eq 5 as a ratio, it is not necessary to employ the absolute values of ϕ_{bound} and ϕ_{free} . Therefore, in these analyses, ϕ_{free} was fixed equal to one, and only ϕ_{bound} and K_a were iterated parameters. To extract binding constants from time-resolved fluorescence data, the ratio of number-average lifetime $\tau_{\text{num}}/\tau_{\text{num},0}$ may be substituted for F/F_0 in eq 5.

Binding of UDG to abasic-site oligos cannot be described by the simple hyperbolic isotherm eq 4 because neither protein nor DNA concentration remains constant over the course of the titration. Therefore, these data were fitted to the general two-state isotherm (42)

$$Y = \frac{([P]_{\Sigma} + [D]_{\Sigma} + K_d) - \sqrt{([P]_{\Sigma} + [D]_{\Sigma} + K_d^{\text{app}})^2 - 4[P]_{\Sigma}[D]_{\Sigma}}}{2[D]_{\Sigma}} \quad (6)$$

where Y is the fraction bound, $[P]_{\Sigma}$ is the total UDG concentration, $[D]_{\Sigma}$ is the total DNA concentration, and K_d^{app} is the apparent dissociation constant for their interaction. The apparent dissociation constant for the interaction of UDG with the abasic site is employed because the contribution of nonspecific UDG–DNA binding to the observed isotherm has not been determined. The bound fraction Y was related to the relative fluorescence F/F_0 according to eq 5. In these analyses, as in the analysis of Ca^{2+} binding, ϕ_{free} was assumed to equal one, and ϕ_{bound} and K_d were iterated parameters.

Fluorescence Quenching Data Analysis. Fluorescence lifetimes from KI quenching titrations were fitted to the Stern–Volmer equation (43) for analysis of collisional quenching

$$\tau_0/\tau = 1 + k_q\tau_0[Q] \quad (7)$$

where τ_0 and τ are the lifetimes in the absence and presence

of quencher, respectively, $[Q]$ is the KI concentration, and k_q is the bimolecular quenching rate constant ($\text{M}^{-1} \text{s}^{-1}$).

RESULTS

The local conformation of DNA abasic sites free in solution may be an important determinant of the specific recognition of such sites by DNA repair proteins. Steady-state fluorescence measurements have suggested that a conformational change occurs upon binding of divalent cations (9). The fluorescence of 2AP opposite an abasic site in dsDNA was observed to increase saturably upon addition of Ca^{2+} , Mg^{2+} , or Mn^{2+} . This change was accompanied by an increase in the accessibility of the fluorophore to added solute quencher (acrylamide), implying that the DNA had undergone a conformational change upon binding of one or more divalent ions. This change in accessibility is consistent with the 2AP opposite the abasic site occupying an extrahelical conformation, although it also conceivably could arise from a more subtle change in the conformation of an intrahelical base.

Further insight into the character and energetics of the conformational states of abasic sites can be obtained from time-resolved fluorescence measurements. Interpretation of these data is greatly enhanced by the model of 2AP quenching in DNA that is developed in the preceding paper in this issue and briefly summarized here. The fluorescence of 2AP is sensitive to both dynamic quenching, which reduces the intensity decay lifetime and the steady-state quantum yield proportionately, and static quenching, which reduces the quantum yield with no effect on the lifetime. Both of these effects arise from interactions between 2AP and the other nucleic acid bases. Dynamic quenching of fluorescence is mediated with high efficiency by collisions between 2AP and each of the other bases, and static quenching is mediated by the formation of aromatic stacking complexes between the bases. The intrinsic efficiency of quenching due to either of these interactions does not vary significantly between the normal DNA bases free in solution. Furthermore, hydrogen bonding does not appear to affect either the lifetime or the quantum yield of 2AP. Therefore, the combination of steady-state and time-resolved data may be interpreted in terms of the interactions of the fluorescent base in DNA with the flanking residues only, giving insight into both local structure and dynamics. Static quenching implies that the local equilibrium conformation of the DNA allows stacking of the bases. Dynamic quenching depends on the rate of base collisions, which will be sensitive both to the equilibrium conformation of the DNA, the mean distance between 2AP, and the neighboring bases, and to DNA dynamics, the characteristics and rates of base motions.

Four dsDNA 19-mers were designed for time-resolved fluorescence experiments. The sequences of these oligos are listed in Table 1. In the text and figures, the oligos are named according to the sequence of their three central base pairs. Two of these oligos contain the THF abasic-site analogue. AFA/TPT contains THF (F) flanked by 5'- and 3'-adenines, opposite 2AP (P) flanked by 5'- and 3'-thymines; this oligo is identical to the one employed in the previous steady-state fluorescence study (9). The second THF-containing oligo contains the central sequence APA/TFT; this oligo is identical to AFA/TPT except that the THF and 2AP are switched

Table 2: Relative Quantum Yields and Number-Average Lifetimes of Oligos

| sample | ϕ_{rel} | τ_{num} (ns) | $\tau_{\text{rel}}/\phi_{\text{rel}}$ | f_{stacked} |
|---------|---------------------|--------------------------|---------------------------------------|----------------------|
| d2AP | 1 ^a | 10.2 ± 0.10 | 1 | 0 |
| AFA/TPT | 0.033 ± 0.003 | 0.72 ± 0.10 | 2.13 ± 0.24 | 0.53 ± 0.12 |
| ATA/TPT | 0.023 ± 0.003 | 0.29 ± 0.10 | 1.22 ± 0.41 | 0.18 ± 0.16 |
| APA/TFT | 0.168 ± 0.003 | 2.22 ± 0.10 | 1.29 ± 0.06 | 0.22 ± 0.02 |
| APA/TTT | 0.015 ± 0.003 | 0.38 ± 0.10 | 2.45 ± 0.52 | 0.59 ± 0.25 |

^a Relative quantum yield of d2AP is taken as one by definition.

between strands. These A:T-rich sequences were employed based on a previous report that such sequences are relatively better substrates for UDG than other sequences are. Comparison between these two sequences enables an investigation of the sequence dependence of the conformation of the abasic site and also allows comparison of the relative quenching effects of adenine and thymine on 2AP. The THF analogue, which is more stable than the 2'-deoxyribose abasic site, was employed for these studies. The THF abasic site demonstrates very similar fluorescence changes upon addition of divalent cation (9). No oligos were examined in which 2AP was situated in other positions relative to the abasic site, e.g., adjacent on the same strand, because no change was observed in the steady-state fluorescence of such oligos upon addition of divalent cations (9). To investigate the differences between abasic-site and undamaged DNA, the undamaged oligos ATA/TPT and APA/TTT also were studied. These two oligos are identical to the two abasic-site oligos except that THF is replaced by thymine.

Static and Dynamic Quenching in DNA. Steady-state and time-resolved fluorescence experiments were performed for each of the four oligos described above to determine the mechanisms of fluorescence quenching that are active in each oligo. The number-averaged lifetime τ_{num} (eq 2) and relative quantum yield ϕ_{rel} observed for each oligo in the absence of divalent cations are summarized in Table 2 (and more detailed discussion of the time-resolved experiments is provided further below). The extent of dynamic quenching (base collisions) is indicated by the decrease in τ_{num} relative to the lifetime of d2AP free in solution. In the absence of static quenching (stacking interactions), ϕ_{rel} will decrease proportionally to τ_{num} ; however, if there is static quenching, there will be a disproportionately greater decrease in ϕ_{rel} than in τ_{num} . The extent of static quenching may be quantified by the ratio $\tau_{\text{rel}}/\phi_{\text{rel}}$ (where τ_{rel} is defined as $\tau_{\text{num}}/\tau_{\text{d2AP}}$). Alternatively, the fraction of oligos in which 2AP is statically quenched may be calculated as $f_{\text{stacked}} = 1 - \phi_{\text{rel}}/\tau_{\text{rel}}$.

The values of ϕ_{rel} , τ_{num} , $\tau_{\text{rel}}/\phi_{\text{rel}}$, and f_{stacked} summarized in Table 2 indicate that 2AP is quenched by both static and dynamic mechanisms to differing extents in all four oligos. These differences imply that the base fluorescence is sensitive to effects both of sequence and of the abasic site. In undamaged oligos, 2AP experiences greater static quenching in the adenine context APA/TTT ($\tau_{\text{rel}}/\phi_{\text{rel}} = 2.45 \pm 0.52$) than in the thymine context ATA/TPT ($\tau_{\text{rel}}/\phi_{\text{rel}} = 1.22 \pm 0.41$), indicating that there is a greater fraction of stacked bases in the former case. This result is consistent with the previously published observation that 2AP is stacked in ss poly-A oligos but not in ss poly-T oligos (44). However, dynamic quenching of 2AP appears to be slightly more efficient in ATA/TPT ($\tau_{\text{num}} = 0.29 \pm 0.1$ ns) than in APA/TTT ($\tau_{\text{num}} = 0.38 \pm 0.1$ ns), suggesting that the frequency

of base collisions may be greater in the former. This difference in collision rates could arise from a difference between oligos in the equilibrium distance separating 2AP and the flanking bases, in the amplitude of local motions, or in both. However, an increase in the average base-base distance should be accompanied by decreased stacking interactions, in disagreement with the observed greater static quenching in APA/TTT. Therefore, the difference in dynamic quenching efficiency suggests that the amplitudes of the local motions giving rise to base collisions are greater in ATA/TPT than in APA/TTT.

The efficiency of dynamic quenching is clearly diminished in both of the abasic-site oligos relative to their undamaged homologues. This decrease in base collisions is consistent with the partial population of a conformational state in which the fluorescent base is flipped out of the DNA helix. As in the undamaged oligos, the efficiency of dynamic quenching is greater for 2AP flanked by thymines ($\tau_{\text{num}} = 0.78 \pm 0.1$ ns for AFA/TPT) than by adenines ($\tau_{\text{num}} = 2.22 \pm 0.1$ ns for APA/TFT). However, the abasic site changes base stacking in opposite ways in the two sequence contexts: the extensive static quenching of 2AP in APA/TTT ($\tau_{\text{rel}}/\phi_{\text{rel}} = 2.45 \pm 0.52$) is relieved in APA/TFT ($\tau_{\text{rel}}/\phi_{\text{rel}} = 1.29 \pm 0.06$), but the moderate (or absent) static quenching of 2AP in ATA/TPT ($\tau_{\text{rel}}/\phi_{\text{rel}} = 1.22 \pm 0.41$) is enhanced in AFA/TPT ($\tau_{\text{rel}}/\phi_{\text{rel}} = 2.31 \pm 0.24$). These results imply that the presence of the abasic site changes the local conformation and dynamics of DNA in a sequence-dependent manner.

Ca²⁺ Titrations. Further information about the conformation of abasic-site DNA can be derived from the perturbation of 2AP fluorescence by the effects of added divalent cations. Because steady-state fluorescence of 2AP previously had been observed to undergo approximately identical changes upon addition of Ca²⁺, Mg²⁺, or Mn²⁺, time-resolved experiments performed with any one of these ions should demonstrate the common response of the abasic site to divalent metal binding. Therefore, in this study divalent ion titrations are performed only with Ca²⁺.

For the abasic-site oligos AFA/TPT and APA/TFT, both steady-state fluorescence intensity and average decay lifetimes increase saturably upon addition of Ca²⁺, as shown in Figure 1. In each case, the relative increase in fluorescence intensity is greater than that in τ_{num} , indicating that both static and dynamic quenching interactions are relieved by addition of divalent ions. The magnitude of the change in τ_{num} is approximately 3.5-fold greater for AFA/TPT than for APA/TFT, and the change in fluorescence intensity is approximately 4-fold greater. The relatively greater increases in fluorescence intensity than in τ_{num} upon Ca²⁺ binding imply a decrease in the stacking interactions that mediate static quenching. For AFA/TPT, f_{stacked} decreases from 0.53 to 0.38; for APA/TFT, f_{stacked} decreases from 0.22 to 0.14. On the basis of the absence of fluorescence intensity changes upon addition of divalent ions to undamaged DNA, Ca²⁺ titrations were not performed for the undamaged oligos ATA/TPT and APA/TTT.

The Ca²⁺-dependent changes in both lifetime and intensity are consistent with reversible binding of divalent metal to DNA. Fitting of the lifetime data to a two-state binding model (eqs 4 and 5) yields equilibrium association constants of 248 ± 20 M⁻¹ and 136 ± 20 M⁻¹ for AFA/TPT and APA/TFT, respectively. Essentially identical binding constants are

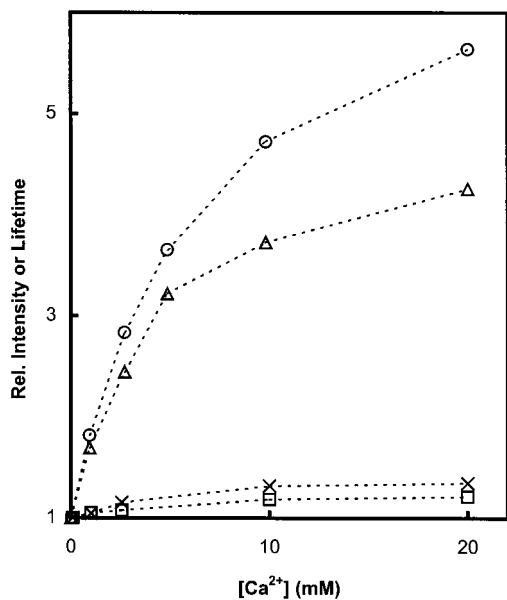


FIGURE 1: Relative fluorescence intensity F/F_0 and relative number-average lifetime τ_{rel} for abasic-site oligos as a function of $[Ca^{2+}]$. The four data series are F/F_0 for AFA/TPT (circles), τ_{rel} for AFA/TPT (triangles), F/F_0 for APA/TFT (x's) and τ_{rel} for APA/TFT (squares). The dashed lines are interpolations between data points only.

derived from the steady-state data. These very similar binding constants agree well with those previously reported (9).

Intensity Decay Kinetics. The fluorescence intensity decays of both the undamaged and the abasic-site oligos at all $[Ca^{2+}]$ are poorly described by a single-exponential model. These decays require sums of three and four exponential terms (eq 1) to achieve a statistically acceptable fit. This multiple-exponential model is only an empirical fit to the data, insofar as no a priori assumption is made as to the mechanism underlying the observed kinetics. The requirement for multiple exponentials in the analysis is consistent with previous reports of the intensity decay kinetics of 2AP in a variety of oligos (45, 46). The values of the lifetimes τ_i , the preexponential factors α_i , and the average lifetimes τ_{num} and τ_{int} are listed in Table 3 for all four of the oligos in the absence of Ca^{2+} and for the two abasic-site oligos in a saturating concentration (20 mM) of Ca^{2+} . As has been mentioned above, τ_{num} is greater for each of the abasic-site oligos than for the respective undamaged oligo. The kinetic parameters in Table 3 reveal that this difference arises from the requirement for a fourth lifetime τ_4 in the intensity decays of the abasic-site oligos, where only three exponential terms are required in the analysis for undamaged DNA. For both AFA/TPT ($\tau_4 = 10.1 \pm 0.1$ ns) and APA/TFT ($\tau_4 = 9.7 \pm 0.1$ ns), this lifetime is significantly longer than any of the other three and does not change significantly between 0 and 20 mM Ca^{2+} . These values do not differ significantly from the single-exponential intensity decay lifetime of free d2AP ($\tau = 10.2 \pm 0.1$ ns).

The preexponential factors α_i vary systematically with increasing $[Ca^{2+}]$, as shown in Figure 2. For both AFA/TPT and APA/TFT, α_4 increases monotonically and saturably with increasing $[Ca^{2+}]$; in the former case, from 0.04 to 0.23, and in the latter case, from 0.02 to 0.10. In a complementary change, the sum of α_1 , α_2 , and α_3 for each oligo decreases over the same range of $[Ca^{2+}]$. The saturable Ca^{2+} -dependent

changes in preexponential factors suggest that τ_4 represents one conformational state, which is thermodynamically favored by divalent ion binding, and the other three lifetimes together represent a second conformer. The absence of the long lifetime from the decays of the undamaged oligos implies that the putative associated conformation is not attained by a significant fraction of these oligos. The relatively long value of τ_4 indicates that in this proposed state 2AP is not accessible to the quenching actions of the other bases. Moreover, the similarity between τ_4 and the free d2AP lifetime suggests that in this state the fluorophore may be completely isolated from the other DNA bases, as would be the case if it were flipped out of the helix. In contrast, the emission from the other conformational state is characterized empirically by three short lifetimes; i.e., it is dynamically quenched and decays with complex kinetics, as expected for an intrahelical base.

For both AFA/TPT and APA/TFT, τ_4 does not change significantly over the full range of Ca^{2+} concentrations. For APA/TFT, there is no significant change in any of the other three lifetimes either. However, for AFA/TPT, τ_1 , τ_2 , and τ_3 each increase moderately with increasing $[Ca^{2+}]$. These changes are approximately monotonic and follow the same saturable dependence on $[Ca^{2+}]$ as do the preexponential factors. Because the iterated parameters in multiple-exponential fits of fluorescence intensity decays are known to be cross-correlated (47), the observation of simultaneous changes in lifetimes and preexponential factors with increasing $[Ca^{2+}]$ raises the possibility that some of those changes may arise from parameter correlation. To reduce the cross-correlation between recovered kinetic parameters, global analysis (39, 40) of decays was performed with the lifetimes forced to assume common values at all $[Ca^{2+}]$. Global analyses in which all four lifetimes are made common to all data sets are statistically acceptable for both oligos, suggesting that the apparent Ca^{2+} -dependent changes in τ_1 , τ_2 , and τ_3 for AFA/TPT in the analyses of individual data sets are not statistically significant. However, the number average of the three short lifetimes τ_{123num} increases monotonically and saturably with increasing Ca^{2+} in both the individual and global analyses for AFA/TPT, as shown in Figure 3. Moreover, the values of τ_{123num} at each $[Ca^{2+}]$ do not differ significantly between individual and global analyses for either oligo. The agreement between values obtained from different analyses implies that τ_{123num} is well-determined, even though the individual α_i 's and τ_i 's that figure into this average lifetime are highly correlated parameters. The Ca^{2+} -dependent increase in τ_{123num} implies that, in addition to shifting the conformational equilibrium toward the state represented by τ_4 , divalent cation binding also may change the structure and dynamics of the other state (in which the opposite base is apparently intrahelical) so as to decrease 2AP quenching. In contrast, the lack of Ca^{2+} -dependence of τ_4 strongly supports the interpretation that this lifetime represents the decay of an extrahelical base that is not subject to quenching by neighboring residues. For APA/TFT, the value of τ_{123num} derived from global analysis decreases slightly upon Ca^{2+} binding. This result implies that the structural and dynamic changes induced in abasic-site DNA by divalent cation binding differ depending on the sequence context in which the damaged site exists.

Table 3: Intensity Decay Parameters for Oligos

| sample | α_1 | α_2 | α_3 | $\alpha_4 (\pm 0.01)^a$ | τ_1 (ns) | τ_2 (ns) | τ_3 (ns) | τ_4 (ns) (± 0.1) ^c | τ_{num} (ns) | τ_{int} (ns) |
|--------------------|------------|------------|------------|-------------------------|---------------|---------------|---------------|--|--------------------------|--------------------------|
| d2APN ^b | | | | 1.000 | | | | 10.2 | 10.2 | 10.2 |
| AFA/TPTN | 0.798 | 0.135 | 0.026 | 0.041 | 0.19 | 0.62 | 2.4 | 10.1 | 0.72 | 6.17 |
| AFA/TPTC | 0.309 | 0.337 | 0.122 | 0.232 | 0.19 | 0.62 | 2.4 | 10.1 | 2.90 | 8.41 |
| ATA/TPTN | 0.473 | 0.447 | 0.080 | | 0.05 | 0.45 | 0.92 | | 0.29 | 0.53 |
| APA/TFTN | 0.186 | 0.225 | 0.574 | 0.016 | 0.13 | 0.93 | 3.2 | 9.7 | 2.22 | 3.41 |
| APA/TFTC | 0.248 | 0.182 | 0.466 | 0.104 | 0.13 | 0.93 | 3.2 | 9.7 | 2.70 | 5.43 |
| APA/TTTN | 0.934 | 0.042 | 0.030 | | 0.19 | 1.2 | 5.1 | | 0.38 | 2.32 |

^a The listed uncertainties in α_4 and τ_4 are estimated from data fitting. Uncertainties are not listed for the other three preexponential factors or lifetimes because these parameters are highly cross-correlated in the analysis. However, the uncertainties in the sum ($\alpha_1 + \alpha_2 + \alpha_3$) and $\tau_{123\text{num}}$ are equal to those in α_4 and τ_4 , respectively (see the text). ^b The letters N and C indicate buffer conditions of 0 mM CaCl₂ and 20 mM CaCl₂, respectively. ^c The goodness-of-fit is not improved for the intensity decays of either of the two undamaged oligos by addition of another exponential term. The values of τ_{num} and τ_{int} are invariant upon addition of subsequent exponential terms for all data sets.

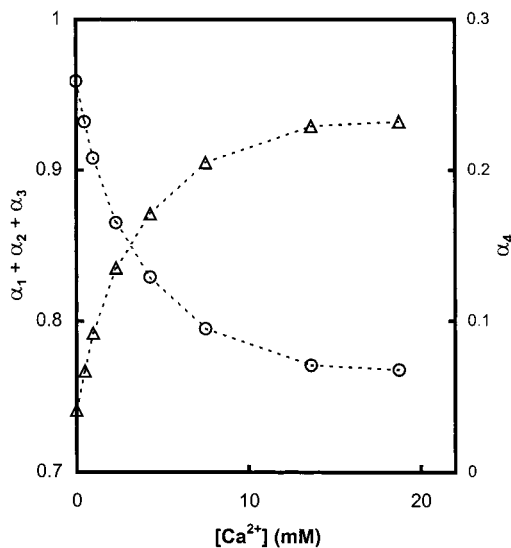


FIGURE 2: Preexponential factors α_i for AFA/TPT as a function of $[\text{Ca}^{2+}]$. The sum $\alpha_1 + \alpha_2 + \alpha_3$ (circles) is plotted relative to the left-hand axis, and α_4 (triangles) is plotted relative to the right-hand axis. The dashed lines are interpolations between data points only.

In summary, the time-resolved fluorescence measurements suggest that divalent ion binding to abasic-site oligos apparently perturbs the equilibrium between two conformational states in which the opposite base is in very different environments. The first state is characterized by efficiently quenched fluorescence emission with complex decay kinetics requiring three exponential terms to fit. The decay kinetics in this state are very similar to those observed in undamaged DNA and are consistent with the expected decay of 2AP in an intrahelical (“closed”) conformation. The second state is characterized by unquenched emission with single-exponential lifetime equal to that of free d2AP. The decay kinetics of the unquenched state are consistent with those expected of 2AP in an extrahelical (“open”) conformation. For AFA/TPT, the average decay lifetime $\tau_{123\text{num}}$ of the closed state increases with Ca^{2+} binding, implying that the bound ion changes the structure or dynamics of this state so as to decrease collisional quenching of 2AP by the flanking bases. For APA/TFT, $\tau_{123\text{num}}$ decreases slightly upon Ca^{2+} binding, implying that cation binding increases 2AP quenching in this oligo. Thus, the changes in structure and dynamics of the closed state due to the bound ion differ depending on the sequence of the oligo. The average lifetime τ_4 of the open state is invariant to $[\text{Ca}^{2+}]$ in both oligos, as would be expected for an extrahelical base. While certain kinetic

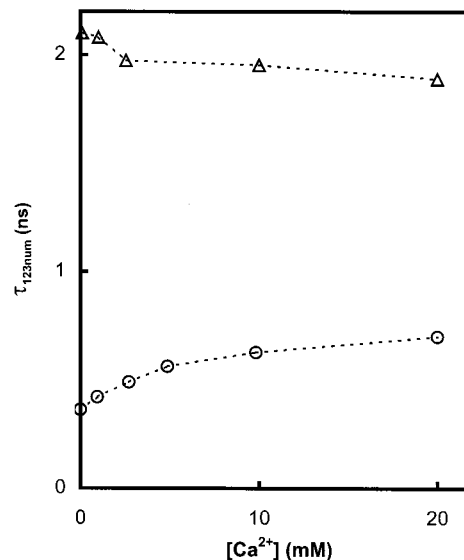


FIGURE 3: Number average of the three shorter lifetimes $\tau_{123\text{num}}$ as a function of $[\text{Ca}^{2+}]$ for AFA/TPT (circles) and APA/TFT (triangles). The dashed lines are interpolations between data points only.

parameters are highly cross-correlated in the data analysis, the fractional populations of the closed ($\alpha_1 + \alpha_2 + \alpha_3$) and open (α_4) states are well-determined, as are their respective lifetimes $\tau_{123\text{num}}$ and τ_4 .

The intensity decays reveal the basis for the much larger Ca^{2+} -dependent increases in τ_{num} and fluorescence intensity (shown in Figure 1) for AFA/TPT than for APA/TFT. For both oligos, the lifetime of the open state is approximately 10 ns. However, for AFA/TPT, the average lifetime $\tau_{123\text{num}}$ of the closed state ranges between 0.3 to 0.7 ns as a function of $[\text{Ca}^{2+}]$; for APA/TFT, $\tau_{123\text{num}}$ is approximately 2 ns. Furthermore, α_4 increases by 0.19 between the Ca^{2+} -free and Ca^{2+} -bound states of AFA/TPT but only increases by 0.08 between the corresponding states of APA/TFT. Thus, the difference in the amplitude of the fluorescence changes shown in Figure 1 arises from the combination of a more quenched closed state and a greater Ca^{2+} -dependent increase in the population of the open state for AFA/TPT than for APA/TFT.

The observation of static quenching (Table 2) in both abasic-site oligos implies that there is actually a third state in which 2AP opposite the abasic site is stacked with the flanking bases. The relief of static quenching upon Ca^{2+} binding (shown in Figure 1) is consistent with a shift in the equilibrium between this stacked state and the open state.

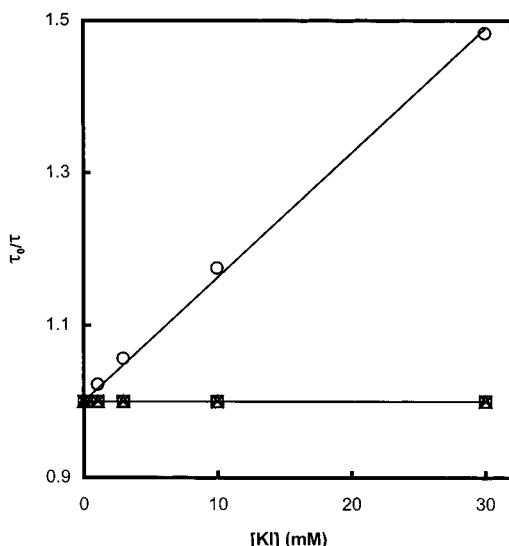


FIGURE 4: Stern–Volmer plot of changes in lifetime components for AFA/TPT as a function of [KI]. The four data series represent the ratio τ_0/τ for each of the four lifetime components τ_1 (triangles), τ_2 (x's), τ_3 (squares), and τ_4 (circles), respectively. The line represents a fit of eq 7 to the data for τ_4 with $k_q = 1.5 \times 10^9 \text{ M}^{-1} \text{ s}^{-1}$ and $\tau_0 = 9.9 \text{ ns}$.

Thus, three conformations of the opposite base can be distinguished by the combination of steady-state and time-resolved fluorescence measurements: intrahelical stacked, intrahelical unstacked, and extrahelical. The fractional population of the first of these states is f_{stacked} (Table 2); the populations of the other two states may be derived by scaling the relative amplitudes $\alpha_1 + \alpha_2 + \alpha_3$ and α_4 by a factor of $(1 - f_{\text{stacked}})$. From these equilibrium populations, the free energy differences between the three states may be determined. For example, for AFA/TPT in the absence of Ca^{2+} , the fractional populations of the stacked, unstacked, and open states are 0.53, 0.45, and 0.02, respectively. Thus, the unstacked state is marginally less stable than the stacked state, and the open state is approximately 2 kcal/mol higher in energy than either. In the presence of saturating Ca^{2+} , the fractional populations are 0.38, 0.48, and 0.14 for stacked, unstacked, and open, respectively. The two intrahelical states remain nearly isoenergetic, but the open state is only 0.7 kcal/mol higher in energy than the others. Thus, Ca^{2+} binding, for which the free energy change is -3.3 kcal/mol , shifts the conformational equilibrium 1.3 kcal/mol toward the open state. The free energy differences between states for APA/TFT in both the presence and absence of Ca^{2+} are on the same order of magnitude as those for AFA/TPT.

KI Quenching. The accessibility of 2AP opposite an abasic site to the solute quencher acrylamide has been shown to increase upon binding of divalent ions by steady-state fluorescence (9). This result is consistent with the shift from closed to open conformational states upon Ca^{2+} binding that is proposed above. To test the assignment of fluorescence lifetimes to conformational states, this solute quenching experiment was repeated by the time-resolved method. This experiment was performed using KI as the added quencher to avoid possible complications associated with binding of acrylamide to DNA and was performed in the presence of saturating Ca^{2+} (30 mM) to maximize the contribution of τ_4 to the signal. Figure 4 is a Stern–Volmer plot of the changes in the individual lifetimes as a function of [KI], which shows

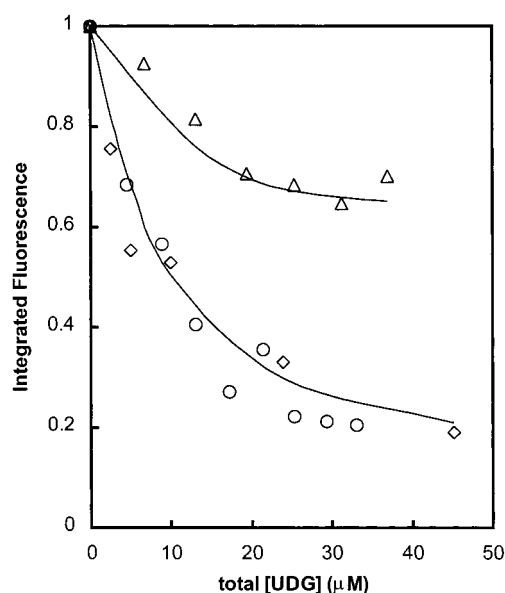


FIGURE 5: Steady-state fluorescence intensity for AFA/TPT as a function of [UDG]. The three series represent one titration performed at 0 mM Ca^{2+} (triangles) and two separate titrations performed at 30 mM Ca^{2+} (circles and diamonds). The [DNA] in each titration is approximately constant. The [DNA] in the titration at 0 mM Ca^{2+} is $16 \mu\text{M}$, and in each of the titrations at 20 mM Ca^{2+} is approximately $6.5 \mu\text{M}$. Each data set is scaled to an initial value of one. The lines represent fits of eq 5 to the data (with Y in eq 5 substituted by eq 6). In the absence of Ca^{2+} , $K_d = 2.9 \mu\text{M}$ [$1.5 \mu\text{M}$, $4.8 \mu\text{M}$], and in the presence of Ca^{2+} , $K_d = 4.2 \mu\text{M}$ [$3.3 \mu\text{M}$, $5.2 \mu\text{M}$]. The numbers in brackets represent the 95% confidence intervals for K_d estimated from the dispersion of experimental data points around the fitted functions.

that τ_4 is significantly more sensitive to the presence of quencher than are the other three lifetimes. While τ_4 is quenched with a bimolecular rate constant of $1.5 \pm 0.1 \times 10^9 \text{ M}^{-1} \text{ s}^{-1}$, the changes in the other three lifetimes are negligible. In a global analysis, these three lifetimes all could be maintained at constant values over the entire range of [KI], implying that they are essentially insensitive to the quencher. However, analyses in which τ_4 is held constant are not statistically acceptable. These results strongly support the model that τ_4 represents the fluorescence decay of an extrahelical base, while the three shorter lifetimes represent the decay of 2AP in an intrahelical conformation.

UDG Binding. In crystal structures of *E. coli* UDG complexed to abasic-site DNA, the base opposite the abasic site is intrahelical (27, 31). Therefore, addition of UDG to abasic-site oligos is expected to shift the population of conformers toward the intrahelical state. For oligos containing 2AP, the fluorescence properties should change to reflect the new conformational equilibrium. Figure 5 shows the fluorescence intensity changes for AFA/TPT as a function of [UDG] in both the presence and absence of divalent cation. For both Ca^{2+} -free and Ca^{2+} -bound oligos, the enzyme causes a saturable decrease in 2AP fluorescence. Fitting of these curves to a general two-state binding model (eq 6) yields apparent equilibrium dissociation constants K_d^{app} of $2.9 \mu\text{M}$ at 0 mM Ca^{2+} and $4.2 \mu\text{M}$ at 18 mM Ca^{2+} . The apparent dissociation constant is employed because the contribution of nonspecific UDG–DNA binding to the observed isotherm has not been determined. These values agree well with those previously determined for this interac-

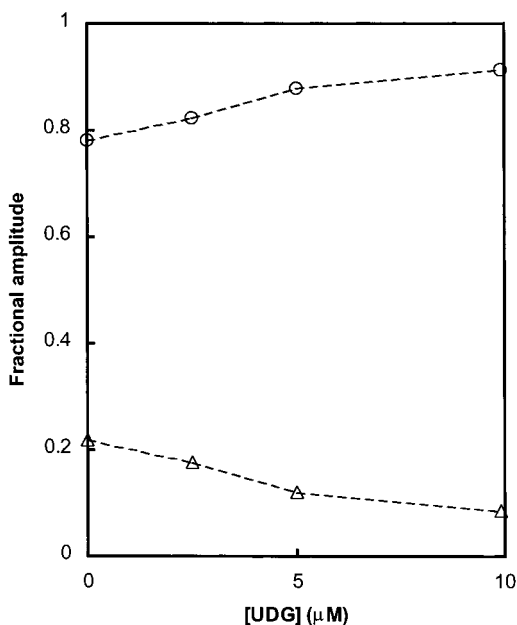


FIGURE 6: Preexponential factors α_i for AFA/TPT as a function of [UDG] at 20 mM Ca^{2+} . The two data series represent $\alpha_1 + \alpha_2 + \alpha_3$ (circles) and α_4 (triangles), respectively. The dashed lines are interpolations between data points only. The [DNA] is approximately constant at 6.5 μM .

tion by other methods. The decrease in fluorescence intensity upon UDG binding is consistent with a shift in the conformational equilibrium toward the more quenched intrahelical state. The amplitude of the UDG-dependent intensity change is greater in the presence of Ca^{2+} , as would be expected because the open state is more populated when the oligo is bound by divalent ion. The negligible difference in UDG–DNA binding constant between Ca^{2+} -free and Ca^{2+} -bound states is consistent with the small changes in equilibrium populations of the various conformers due to divalent cation binding.

The changes in intensity decay kinetics agree with the proposed shift toward the closed state upon binding of UDG. Figure 6 shows the changes in $\alpha_1 + \alpha_2 + \alpha_3$ and α_4 with increasing UDG at 18 mM Ca^{2+} . The fractional amplitudes of the three short-lifetime components increase, and that of the long lifetime decreases, consistent with a shift toward the closed state. The values of all four lifetimes show no change over the protein concentration range shown. The data in Figure 6 are shown for a maximum [UDG] of 10 μM , because the protein fluorescence becomes a significant interference above this value. UDG has six tryptophan (Trp) residues, several of which are buried in the hydrophobic core of the protein (48). The absorption spectra of such buried Trp residues are characteristically shifted to longer wavelengths, so that even at 309 nm their extinction is significant (43). The combination of this red-shifted absorption, the low quantum yield of the oligo (Table 2), and the relatively high quantum yield of UDG (data not shown) ensure that it is impossible to avoid the protein fluorescence at higher enzyme concentrations. Consequently, the intensity decays cannot be interpreted solely in terms of 2AP fluorescence. It should be noted that UDG fluorescence does not affect the interpretation of the steady-state intensity changes shown in Figure 5, because these data are excited at 325 nm, where

the Trp absorption is much less than at 309 nm (the excitation wavelength for the time-resolved experiment).

In summary, the UDG-dependent changes in fluorescence intensity and decay kinetics are consistent with an increase in the population of the closed state, in agreement with the conformation observed in crystal structures. Interestingly, the changes in τ_{num} with increasing [UDG] are directly proportional to the steady-state intensity changes. Therefore, there is no increase in static quenching upon UDG binding, implying that the protein favors the closed, unstacked state of the opposite base.

DISCUSSION

The recognition of DNA damage may depend on both the unusual conformation (structure) and the susceptibility to particular deformations (dynamics) of the damaged site. In this study, we have demonstrated on the basis of steady-state and time-resolved fluorescence properties that abasic-site DNA exists in a mixture of conformational states free in solution that differ in the location of the opposite base. The equilibrium between the open, closed stacked, and closed unstacked states of the opposite base can be detected by the differing fluorescence properties of 2AP in this position. The open state is not quenched by collisions with the neighboring bases, but is accessible to the solute quencher KI. The closed unstacked state is quenched by the DNA bases, but not by KI. The closed stacked state is statically quenched by base stacking interactions. The characteristics of the three conformational states are elucidated by perturbing the equilibrium between them upon addition of Ca^{2+} or UDG.

The observation of conformational heterogeneity of the free abasic site has significant implications for the specific recognition of this site by repair enzymes. The DNA deformations required by these enzymes in complex with abasic-site DNA are severe and in the case of endo IV includes opposite-base flipping (29). The free energy differences between open and closed states are fairly small: less than 1 kcal/mol in the presence of saturating divalent ion. Therefore, only a small energetic penalty is required for a repair enzyme to flip the base opposite the abasic site either in or out of the helix. An enzyme could drive the DNA to its preferred conformation with little difficulty, regardless of whether that conformation was more similar to the open or closed states of the free DNA. In contrast, the absence of the open state in the undamaged oligos implies that the energetic cost of deforming undamaged DNA is relatively greater than for abasic-site DNA. Therefore, the conformational heterogeneity observed in this study suggests roles for both equilibrium structural deformation and enhanced dynamic deformability in the recognition of abasic sites by repair enzymes.

The assignment of intensity decay lifetimes to conformational states is enabled by divalent cation-induced changes in the populations of these states. The observation of these effects raises the question of whether divalent cations might play some role in regulating the interactions of repair proteins with abasic-site DNA. We consider such a regulatory role unlikely, for two reasons. First, the shifts in conformational equilibria due to Ca^{2+} binding are fairly small and do not alter the primary fact that the three conformers are fairly close to each other in energy. For example, the fractional

population of the open state of AFA/TPT increases only from 0.04 to 0.23 upon Ca^{2+} binding, and consequently the affinity of UDG for the abasic site is practically unchanged. Second, in a living cell, the DNA will in all probability be bound constitutively by Mg^{2+} , which is present at a physiological concentration of approximately 30 mM (49). Even given the presence of numerous competing Mg^{2+} binding sites in the cell, this concentration is probably sufficient to saturate any available abasic sites. Consequently, changes in total divalent cation concentration, such as in Ca^{2+} bursts, are not expected to change the conformational equilibrium of the already saturated abasic site significantly.

In addition to shifting the conformational equilibrium toward the open state, Ca^{2+} binding also causes a change in the structure and/or dynamics of the closed state. The nature of this change depends on the sequence context of the abasic site: in AFA/TPT the dynamic quenching of 2AP decreased significantly, while in APA/TFT it slightly increased. These changes in quenching could arise from a change in equilibrium structure, a change in the amplitudes and character of base motions, or a combination of the two. A recent computational molecular dynamics study of an oligo with sequence similar to AFA/TPT found that Mg^{2+} binding both bent and rigidified the DNA in the vicinity of the abasic site (50). Therefore, both structural and dynamic changes appear to contribute to this effect.

In undamaged DNA, 2AP is found to exist in a mixture of stacked and unstacked states. The fractional population of the stacked state differs in the two oligos examined, implying that the structure of undamaged DNA varies locally with sequence. Furthermore, the efficiency of dynamic quenching also differs between these two oligos but is not proportional to the static quenching. The lack of correlation between stacking and base collision rates provides strong evidence in favor of the proposition that the dynamics of DNA varies locally with base sequence. The full extent of this variation cannot be determined without measuring the static and dynamic quenching of 2AP in a number of sequence contexts. It should be noted that the two sequences employed in this study are both fairly unusual. In APA/TTT, the fluorophore is embedded in the middle of an A-tract nine residues in length; A-tract sequences have been reported to have an intrinsically curved structure (51). In ATA/TPT, the 2AP:T base pair forms the junction between two A-tracts three and five base pairs in length, respectively; such junctions also could possess unique properties. Studies are underway to characterize the sequence dependence of dynamic and static quenching interactions in a systematic manner, and to relate these spectroscopic properties to other measures of sequence-dependent DNA structure and dynamics.

The complex intensity decay kinetics of 2AP in both the closed state of abasic-site DNA and in undamaged DNA arise from some mechanism that is currently unknown. Although these decays are empirically fit by an sum of three exponentials, it is quite possible that the true kinetic model takes a very different functional form. In the preceding paper in this issue, it is shown that high concentrations of nucleosides can induce complex "multiexponential" intensity decay kinetics for 2AP free in solution. These data are consistent with a model of collisional quenching in the limit in which transient diffusional effects become important. On the basis

of these results, we speculate that the complex decays of 2AP in DNA may arise from a mechanism in which the rate of quenching due to base collisions is modulated by the rapid internal dynamics of the DNA. As discussed in the preceding paper in this issue, it is possible that considerably more information about DNA dynamics is present in the decay data than we currently utilize.

Using 2AP fluorescence, it is possible to identify and characterize molecular states that are difficult to detect by other methods (e.g., solution NMR) and to quantify the relative populations and energies of these states with high precision. It is apparent that the bulk of this information can be obtained only through the combination of steady-state and time-resolved fluorescence measurements. It should now be possible to apply this algorithm to obtain detailed dynamic and thermodynamic information about many DNA and RNA sites of biological interest.

ACKNOWLEDGMENT

The authors gratefully acknowledge Gintaras Deikus for sharing unpublished data and thank William R. Laws and Elena Rusinova for invaluable discussions. Preliminary results from this study were presented at the 1999 Weber Symposium on Innovative Fluorescence Methodologies in Biochemistry and Medicine and at the 2000 Annual Meeting of the Biophysical Society.

REFERENCES

- Lindahl, T. (1993) *Nature* 362, 709–15.
- Mol, C. D., Parikh, S. S., Putnam, C. D., Lo, T. P., and Tainer, J. A. (1999) *Annu. Rev. Biophys. Biomol. Struct.* 28, 101–28.
- Lindahl, T. (1990) *Mutat. Res.* 238, 305–11.
- Kingma, P. S., Corbett, A. H., Burcham, P. C., Marnett, L. J., and Osheroff, N. (1995) *J. Biol. Chem.* 270, 21441–4.
- Krokan, H. E., Standal, R., and Slupphaug, G. (1997) *Biochem. J.* 325, 1–16.
- Parikh, S. S., Mol, C. D., and Tainer, J. A. (1997) *Structure* 5, 1543–50.
- Parikh, S. S., Mol, C. D., Hosfield, D. J., and Tainer, J. A. (1999) *Curr. Opin. Struct. Biol.* 9, 37–47.
- Xing, D., Dorr, R., Cunningham, R. P., and Scholes, C. P. (1995) *Biochemistry* 34, 2537–44.
- Stivers, J. T. (1998) *Nucleic Acids Res.* 26, 3837–44.
- Erzberger, J. P., Barsky, D., Schärer, O. D., Colvin, M. E., and Wilson, D. M., 3rd. (1998) *Nucleic Acids Res.* 26, 2771–8.
- Parikh, S. S., Mol, C. D., Slupphaug, G., Bharati, S., Krokan, H. E., and Tainer, J. A. (1998) *EMBO J.* 17, 5214–26.
- Mol, C. D., Kuo, C. F., Thayer, M. M., Cunningham, R. P., and Tainer, J. A. (1995) *Nature* 374, 381–6.
- Gorman, M. A., Morera, S., Rothwell, D. G., de La Fortelle, E., Mol, C. D., Tainer, J. A., Hickson, I. D., and Freemont, P. S. (1997) *EMBO J.* 16, 6548–58.
- Cuniasse, P., Fazakerley, G. V., Guschlbauer, W., Kaplan, B. E., and Sowers, L. C. (1990) *J. Mol. Biol.* 213, 303–14.
- Cuniasse, P., Sowers, L. C., Eritja, R., Kaplan, B., Goodman, M. F., Cognet, J. A., LeBret, M., Guschlbauer, W., and Fazakerley, G. V. (1987) *Nucleic Acids Res.* 15, 8003–22.
- Kalnik, M. W., Chang, C. N., Grollman, A. P., and Patel, D. J. (1988) *Biochemistry* 27, 924–31.
- Kalnik, M. W., Chang, C. N., Johnson, F., Grollman, A. P., and Patel, D. J. (1989) *Biochemistry* 28, 3373–83.
- Withka, J. M., Wilde, J. A., Bolton, P. H., Mazumder, A., and Gerlt, J. A. (1991) *Biochemistry* 30, 9931–40.
- Singh, M. P., Hill, G. C., Peoc'h, D., Rayner, B., Imbach, J. L., and Lown, J. W. (1994) *Biochemistry* 33, 10271–85.

20. Goljer, I., Kumar, S., and Bolton, P. H. (1995) *J Biol. Chem.* 270, 22980–7.
21. Coppel, Y., Constant, J. F., Coulombeau, C., Demeunynck, M., Garcia, J., and Lhomme, J. (1997) *Biochemistry* 36, 4831–43.
22. Coppel, Y., Berthet, N., Coulombeau, C., Garcia, J., and Lhomme, J. (1997) *Biochemistry* 36, 4817–30.
23. Beger, R. D., and Bolton, P. H. (1998) *J. Biol. Chem.* 273, 15565–73.
24. Jourdan, M., Garcia, J., Defrancq, E., Kotera, M., and Lhomme, J. (1999) *Biochemistry* 38, 3985–95.
25. Lin, Z., Hung, K. N., Grollman, A. P., and de los Santos, C. (1998) *Nucleic Acids Res.* 26, 2385–91.
26. Wang, K. Y., Parker, S. A., Goljer, I., and Bolton, P. H. (1997) *Biochemistry* 36, 11629–39.
27. Slupphaug, G., Mol, C. D., Kavli, B., Arvai, A. S., Krokan, H. E., and Tainer, J. A. (1996) *Nature* 384, 87–92.
28. Hollis, T., Ichikawa, Y., and Ellenberger, T. (2000) *EMBO J.* 19, 758–66.
29. Hosfield, D. J., Guan, Y., Haas, B. J., Cunningham, R. P., and Tainer, J. A. (1999) *Cell* 98, 397–408.
30. Mol, C. D., Izumi, T., Mitra, S., and Tainer, J. A. (2000) *Nature* 403, 451–6.
31. Parikh, S. S., Walcher, G., Jones, G. D., Slupphaug, G., Krokan, H. E., Blackburn, G. M., and Tainer, J. A. (2000) *Proc. Natl. Acad. Sci. U.S.A.* 97, 5083–8.
32. Vassylyev, D. G., Kashiwagi, T., Mikami, Y., Ariyoshi, M., Iwai, S., Ohtsuka, E., and Morikawa, K. (1995) *Cell* 83, 773–82.
33. Latham, K. A., and Lloyd, R. S. (1994) *Ann. N. Y. Acad. Sci.* 726, 181–96; discussion 196–7.
34. Driscoll, S. L., Hawkins, M. E., Balis, F. M., Pfleiderer, W., and Laws, W. R. (1997) *Biophys. J.* 73, 3277–86.
35. Albert, A., and Taguchi, H. (1973) *J. Chem. Soc. (Perkins Trans.)* 2, 1101–1103.
36. Waxman, E., Rusinova, E., Hasselbacher, C. A., Schwartz, G. P., Laws, W. R., and Ross, J. B. (1993) *Anal. Biochem.* 210, 425–8.
37. Grinvald, A., and Steinberg, I. Z. (1974) *Anal. Biochem.* 59, 583–598.
38. Bevington, P. R. (1969) *Data Reduction and Error Analysis for the Physical Sciences*, McGraw-Hill, New York.
39. Beechem, J. M., Knutson, J. R., Ross, J. B. A., Turner, B. W., and Brand, L. (1983) *Biochemistry* 22, 6054–6058.
40. Knutson, J. R., Beechem, J. M., and Brand, L. (1983) *Chem. Phys. Lett.* 102, 501–507.
41. Badaea, M. G., and Brand, L. (1979) *Methods Enzymol.* 61, 378–425.
42. Wyman, J., and Gill, S. J. (1990) *Binding and Linkage: Functional Chemistry of Biological Macromolecules*, University Science Books, Mill Valley, California.
43. Lakowicz, J. R. (1999) *Principles of Fluorescence Spectroscopy*, 2nd ed., Kluwer Academic/Plenum Publishers, New York.
44. Xu, D. G., and Nordlund, T. M. (2000) *Biophys. J.* 78, 1042–58.
45. Guest, C. R., Hochstrasser, R. A., Sowers, L. C., and Millar, D. P. (1991) *Biochemistry* 30, 3271–9.
46. Nordlund, T. M., Andersson, S., Nilsson, L., Rigler, R., Graslund, A., and McLaughlin, L. W. (1989) *Biochemistry* 28, 9095–103.
47. Johnson, M. L., and Faunt, L. M. (1992) *Methods Enzymol.* 210, 1–37.
48. Drohat, A. C., Xiao, G., Tordova, M., Jagadeesh, J., Pankiewicz, K. W., Watanabe, K. A., Gilliland, G. L., and Stivers, J. T. (1999) *Biochemistry* 38, 11876–86.
49. Berne, R. M., and Levy, M. N. (1993) *Physiology*, 3rd ed., Mosby-Year Book, St. Louis.
50. Deikus, G., Ross, J. B. A., and Osman, R. (2000) *Biophys. J.* 78, 170A.
51. Crothers, D. M., Haran, T. E., and Nadeau, J. G. (1990) *J. Biol. Chem.* 265, 7093–6.

BI001665G